THE JOURNAL OF PHYSICAL CHEMISTRY LETTERS
A JOURNAL OF THE AMERICAN CHEMICAL SOCIETY

pubs.acs.org/JPCL

Letter

An Accurate Linearized Semiclassical Approach for Calculating Cavity-Modified Charge Transfer Rate Constants

Maximilian A. C. Saller,[†] Yifan Lai,[†] and Eitan Geva*

Cite This: *J. Phys. Chem. Lett.* 2022, 13, 2330−2337

Read Online

ACCESS | Metrics & More | Article Recommendations | Supporting Information

ABSTRACT: We show that combining the linearized semiclasscial approximation with Fermi's golden rule (FGR) rate theory gives rise to a general-purpose cost-effective and scalable computational framework that can accurately capture the cavity-induced rate enhancement of charge transfer reactions that occurs when the molecular system is placed inside a microcavity. Both partial linearization with respect to the nuclear and photonic degrees of freedom and full linerization with respect to nuclear, photonic, and electronic degrees of freedom (the latter within the mapping Hamiltonian approach) are shown to be highly accurate, provided that the Wigner transforms of the product (WoP) of operators at the initial time is not replaced by the product of their Wigner transforms. We also show that the partial linearization method yields the quantum-mechanically exact cavity-modified FGR rate constant for a model system in which the donor and acceptor potential energy surfaces are harmonic and identical except for a shift in the equilibrium energy and geometry, if WoP is applied.

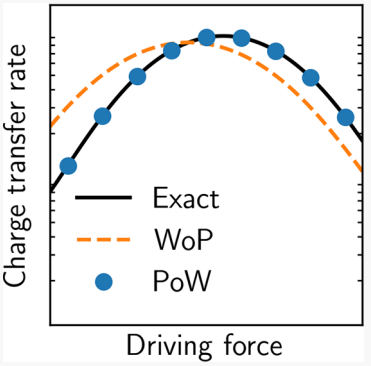

The use of light−matter interactions to control chemical reactions has long been of considerable interest to physical chemists.[1−11] Recent experiments have demonstrated the ability to do so by taking advantage of strong[12−17] and ultrastrong[18−21] coupling between the optical modes of electromagnetic microcavities[22−25] and the electronic and vibrational degrees of freedom (DOF) of molecular matter placed inside the cavity. There is considerable interest in utilizing this coupling to control a variety of chemical and physical processes, including energy and charge transfer, photochemistry and catalysis, and manipulating optical and electrical properties, the nonlinear optical response, and reactivity.[16,18,26−61]

These experimental advances call for the development of accurate and cost-effective computational methods for simulating the dynamics of molecular matter inside cavities. Quantum-mechanically exact methods, while often feasible for the model systems typically studied in quantum optics,[25,62−66] suffer from prohibitive exponential scaling with system size and complexity and are therefore not feasible for most molecular systems of chemical and biological interest. Modeling the dynamics of such systems therefore requires approximate methods that can accurately capture the effect of coupling to cavity modes.

Methods based on the linearized semiclassical (LSC) approximation[67−71] represent one such promising approach for modeling cavity-modified chemical dynamics. Within this approach, the LSC approximation can be applied to just the non-electronic DOF, which is known as partial linearization,[70,72−81] or to both the non-electronic and electronic DOF, known as full linearization.[71] Full linearization is typically based on representing the electronic DOF in terms of mapping variables[82−84] and leads to a family of LSC-based quasiclassical mapping Hamiltonian (QC/MH) methods.[67,68,70,71,85−104]

In our previous work, we have demonstrated that the fully linearized modified LSC (mLSC) QC/MH method, which is based on using improved population operators,[94,95] can yield reasonably accurate results for the quantum dynamics of matter-in-cavity systems.[61] In this work, we demonstrate the ability of both fully and partially linearized LSC-based methods to reproduce the cavity-induced rate enhancement of charge transfer (CT) reactions, in the context of Fermi's golden rule (FGR) rate theory. We demonstrate our LSC-based approach on a benchmark model of CT in a cavity,[105] recently studied using a nonadiabatic ring polymer molecular dynamics (NRPMD) approach.[106−108] We are able to reproduce the enhancement in CT rate due to the cavity using the fully linearized form to a high degree of accuracy. We additionally show that the partially linearized LSC approach yields the quantum-mechanically exact cavity-enhanced FGR CT rate constants for this system.

In what follows, we consider the benchmark model Hamiltonian of a molecular system undergoing CT while being coupled to a single cavity mode that was recently studied by Huo et al.[105] We adopt the same parameters and

Received: January 14, 2022
Accepted: March 2, 2022

https://doi.org/10.1021/acs.jpclett.2c00122
J. Phys. Chem. Lett. 2022, 13, 2330−2337

discretization scheme to allow for easy comparison to the results obtained via NRPMD, as reported in ref 105. A detailed summary of the parameters, discretization scheme, and initial conditions employed in this work can be found in section S1 of the Supporting Information.

The full light−matter Hamiltonian is given by

$$\hat{H} = -\varepsilon|\mathrm{A}\rangle\langle\mathrm{A}| + \Delta(|\mathrm{D}\rangle\langle\mathrm{A}| + |\mathrm{A}\rangle\langle\mathrm{D}|) + \frac{P_s^2}{2M_s} + \sum_{\alpha}\frac{1}{2}M_s\omega_s^2(\hat{R}_s - R_{\alpha,0})^2|\alpha\rangle\langle\alpha| + \hat{H}_{\mathrm{SB}} + \hat{H}_{\mathrm{F}} \quad (1)$$

where $-\varepsilon = \Delta G$ is the driving force of the CT reaction, $\Delta = 5$ meV is the electronic coupling coefficient between the diabatic donor, $|\mathrm{D}\rangle$, and acceptor, $|\mathrm{A}\rangle$, states, and $\alpha \in \{\mathrm{D}, \mathrm{A}\}$.

R_s, P_s, and $M_s = 0.265$ ps^2 and a $\omega_s = 9.5$ meV correspond to the position, momentum, mass, and frequency, respectively, of the primary solvent DOF that is directly coupled to the electronic DOF.

$R_{\mathrm{D},0} = 0$ and $R_{\mathrm{A},0} = \sqrt{2\lambda/f_0}$ correspond to the equilibrium geometry displacements of this DOF in the donor and acceptor states, respectively. Here, $\lambda = 950$ meV is the reorganization energy and $f_0 = 55.7$ is the force constant. $\hat{H}_{\mathrm{SB}}$ corresponds to the Hamiltonian of the bath of secondary solvent DOF, which are coupled to the primary solvent DOF, and is given by

$$\hat{H}_{\mathrm{SB}} = \sum_{j=1}^{B}\left[\frac{\hat{P}_j^2}{2M_j} + \frac{M_j\omega_j^2}{2}\left(\hat{R}_j - \frac{c_j}{M_j\omega_j^2}\hat{R}_s\right)^2\right] \quad (2)$$

where $B = 100$ is the number of bath DOFs. The position, momentum, and mass of the jth bath mode are given by R_j, P_j, and $M_j = M_s$, respectively, and the frequency and coupling coefficient, ω_j and c_j, are obtained from discretizing an ohmic spectral density of the form

$$J(\omega) = \frac{\pi}{2}\sum_{j=1}^{B}\frac{c_j^2}{M_j\omega_j}\delta(\omega - \omega_j) = \eta\omega e^{-\omega/\omega_c} \quad (3)$$

where $\omega_c = 9.5$ meV and $\eta = 1.066 \times 10^6$ au are the characteristic frequency of the bath and the friction coefficient, respectively. Following ref 105, we adopt the discretrization scheme from ref 109. Finally, $\hat{H}_{\mathrm{F}}$ is the field−matter Hamiltonian that is given by

$$\hat{H}_{\mathrm{F}} = \hbar\omega_{\mathrm{F}}a_{\mathrm{F}}^{\dagger}a_{\mathrm{F}} + \hbar g_{\mathrm{F}}(|\mathrm{D}\rangle\langle\mathrm{A}| + |\mathrm{A}\rangle\langle\mathrm{D}|)(a_{\mathrm{F}}^{\dagger} + a_{\mathrm{F}}) \quad (4)$$

where ω_{F} is the frequency of the single-field mode coupled to the electronic DOF of the material system and $a_{\mathrm{F}}^{\dagger}$ and a_{F} are the corresponding photonic creation and annihilation operators, respectively. The field−matter coupling strength is given by

$$\hbar g_{\mathrm{F}} = \sqrt{\frac{\hbar\omega_{\mathrm{F}}}{2\varepsilon_0 L}}\mu_{\mathrm{DA}} \quad (5)$$

where ε_0 and L are the vacuum permittivity and the length of the cavity, respectively, and $\mu_{\mathrm{DA}} = \mu_{\mathrm{AD}}$ is the electronic transition dipole moment. Following ref 105, we present results that correspond to a temperature of 300 K and for two different sets of field parameters, which correspond to the CT process following rate kinetics,[105] which will be termed model I and model II (see Table 1).

We will briefly discuss the theoretical framework that leads to the well-known equilibrium FGR expression for the rate constant and highlight two different strategies for calculating it within the LSC approximation.

Table 1. Field Mode Frequency and Light−Matter Coupling Parameters for Two CTs in Cavity Hamiltonians under Consideration

	model I	model II
$\hbar g_{\mathrm{F}}$	3 meV	5 meV
$\hbar\omega_{\mathrm{F}}$	10 meV	200 meV

The nuclear and photonic DOF are assumed to initially be in thermal equilibrium at the donor state, such that

$$\hat{\rho}(0) = \hat{\rho}_{\mathrm{D}}^{\mathrm{eq}} \otimes |\mathrm{D}\rangle\langle\mathrm{D}| \quad (6)$$

where

$$\hat{\rho}_{\mathrm{D}}^{\mathrm{eq}} = \frac{e^{-\beta\hat{H}_{\mathrm{D}}}}{\mathrm{Tr}_{\mathrm{NP}}(e^{-\beta\hat{H}_{\mathrm{D}}})} \quad (7)$$

where $\beta = 1/k_{\mathrm{B}}T$, $\hat{H}_{\mathrm{D}} = \langle\mathrm{D}|\hat{H}|\mathrm{D}\rangle$, and $\mathrm{Tr}_{\mathrm{NP}} = \mathrm{Tr}_{\mathrm{N}}\mathrm{Tr}_{\mathrm{P}}$, were Tr_{N} is the partial trace over the nuclear DOF and Tr_{P} is the partial trace over the photonic DOF. The donor-to-acceptor equilibrium FGR rate constant, k, can be obtained from second-order perturbation theory by treating the off-diagonal electronic coupling term, given by

$$\hat{H}_{\mathrm{I}} = \Delta(|\mathrm{D}\rangle\langle\mathrm{A}| + |\mathrm{A}\rangle\langle\mathrm{D}|) + \hbar g_{\mathrm{F}}(a_{\mathrm{F}}^{\dagger} + a_{\mathrm{F}})(|\mathrm{D}\rangle\langle\mathrm{A}| + |\mathrm{A}\rangle\langle\mathrm{D}|)$$

as a small perturbation to $\hat{H}_0 = \hat{H} - \hat{H}_{\mathrm{I}}$, the zeroth-order Hamiltonian. The resulting expression for the equilibrium FGR rate constant is given by

$$k = \int_{-\infty}^{\infty}\mathrm{d}t C_{\mathrm{FGR}}(t) \quad (8)$$

where the FGR correlation function is given by

$$C_{\mathrm{FGR}}(t) = \mathrm{Tr}(\hat{\rho}_{\mathrm{D}}^{\mathrm{eq}} \otimes |\mathrm{D}\rangle\langle\mathrm{D}|e^{i\hat{H}_0 t}\hat{H}_{\mathrm{I}}e^{-i\hat{H}_0 t}\hat{H}_{\mathrm{I}}) \quad (9)$$

We note that the trace in eq 9 is the full trace, i.e., over the electronic, nuclear, and photonic DOF ($\mathrm{Tr} = \mathrm{Tr}_{\mathrm{E}}\,\mathrm{Tr}_{\mathrm{N}}\,\mathrm{Tr}_{\mathrm{P}}$).

The next step is to evaluate the FGR correlation function, eq 9, within the framework of the LSC approximation.[67,68,70,71] Because the LSC approximation can be applied either to just the non-electronic (i.e., nuclear and photonic) DOF (termed partial linearization) or to both the electronic and the non-electronic DOF (termed full linearization), this gives rise to two different LSC-based approaches for calculating the FGR rate constant in eq 8,[70,73,79−81,110] which we will discuss below in more detail.

Partial linearization[70,73,79−81,110] involves performing the trace over the electronic DOF (Tr_{E}) in eq 9 explicitly, thereby casting the FGR correlation function in the following form:

$$C_{\mathrm{FGR}}(t) = \mathrm{Tr}_{\mathrm{NP}}[\hat{H}_{\mathrm{I,AD}}\hat{\rho}_{\mathrm{D}}^{\mathrm{eq}}e^{i\hat{H}_{\mathrm{D}}t}\hat{H}_{\mathrm{I,DA}}e^{-i\hat{H}_{\mathrm{A}}t}] \quad (10)$$

where $\hat{H}_{\mathrm{I},jk} = \langle j|\hat{H}_{\mathrm{I}}|k\rangle$. We note that $\mathrm{Tr}_{\mathrm{NP}} = \mathrm{Tr}_{\mathrm{N}}\,\mathrm{Tr}_{\mathrm{P}}$ in eq 10 corresponds to the trace over the nuclear and photonic (i.e., non-electronic) DOF. Applying the LSC approximation to the non-electronic DOF then yields the following approximate expression for the FGR correlation function:

https://doi.org/10.1021/acs.jpclett.2c00122
J. Phys. Chem. Lett. 2022, 13, 2330−2337

$$C_{\mathrm{FGR}}(t) \approx \frac{1}{(2\pi)^{B+2}} \iint \mathrm{d}\mathbf{R}\, \mathrm{d}\mathbf{P} [\hat{H}_{\mathrm{I,AD}} \hat{\rho}_{\mathrm{D}}^{\mathrm{eq}}]^{\mathrm{W}} (\mathbf{R}(0), \mathbf{P}(0)) [\hat{H}_{\mathrm{I,DA}}]^{\mathrm{W}} (\mathbf{R}(t), \mathbf{P}(t)) \exp\left\{ \frac{\mathrm{i}}{\hbar} \int_0^t \mathrm{d}s U(\mathbf{R}(s)) \right\} \tag{11}$$

where $\mathbf{R} = (R_1, ..., R_B, R_F)$ and $\mathbf{P} = (P_1, ..., P_B, P_F)$, where $\hat{R}_F = \sqrt{\frac{\hbar}{2\omega_F}} (\hat{a}_F + \hat{a}_F^\dagger)$ and $\hat{P}_F = -i\sqrt{\frac{\hbar\omega_F}{2}} (\hat{a}_F - \hat{a}_F^\dagger)$ are the photonic coordinate and momentum operators, respectively; $U = V_D - V_A$ is the energy gap between donor and acceptor potential energy surfaces (PESs); $\mathbf{R}(t)$ and $\mathbf{P}(t)$ are obtained via classical propagation on the average PES, $\bar{V} = (V_D + V_A)/2$, with $\mathbf{R}(0)$ and $\mathbf{P}(0)$ as the initial conditions; and $[\cdot]^{\mathrm{W}}$ denotes the Wigner transform, given by

$$[\hat{O}]^{\mathrm{W}} (\mathbf{R}, \mathbf{P}) = \int \mathrm{d}\mathbf{X} e^{\mathrm{i}\mathbf{X}\mathbf{P}} \left\langle \mathbf{R} - \frac{\mathbf{X}}{2} \middle| \hat{O} \middle| \mathbf{R} + \frac{\mathbf{X}}{2} \right\rangle \tag{12}$$

for any operator $\hat{O}$. A detailed derivation of eq 11 can be found in refs 71 and 73. We note that, because of the harmonic nature of the electronic potential energy surfaces (eq 1) both the quantum-mechanically exact FGR correlation function (eq 10) and the corresponding partially linearized LSC approximation (eq 11) can be obtained in closed form via Gaussian integration,[73,80] which is shown in section S2 of the Supporting Information. Importantly, the partial linearization can be shown to reproduce the quantum-mechanically exact FGR correlation function for harmonic molecular Hamiltonians such as the one employed in this paper, both in the cavity-free[70,73] case and in the cavity-modified case. The latter is shown in section S3 of the Supporting Information.

Full linearization[70] casts the FGR correlation function (eq 9) in the following form:

$$C_{\mathrm{FGR}}(t) = \mathrm{Tr}[\hat{\rho}_{\mathrm{D}}^{\mathrm{eq}} \otimes |\mathrm{A}\rangle\langle \mathrm{D}| e^{\mathrm{i}\hat{H}_0 t} \hat{H}_{\mathrm{I,DA}} \otimes |\mathrm{D}\rangle\langle \mathrm{A}| e^{-\mathrm{i}\hat{H}_0 t} \hat{H}_{\mathrm{I,AD}}] \tag{13}$$

Applying the LSC approximation to fully linearize this expression[70] yields

$$C_{\mathrm{FGR}}(t) \approx \frac{1}{(2\pi)^{B+4}} \int\int\int\int \mathrm{d}\mathbf{x}\, \mathrm{d}\mathbf{p}\, \mathrm{d}\mathbf{R}\, \mathrm{d}\mathbf{P} [\hat{H}_{\mathrm{I,AD}} \hat{\rho}_{\mathrm{D}}^{\mathrm{eq}}]^{\mathrm{W}} (\mathbf{R}(0), \mathbf{P}(0)) \times M_{\mathrm{AD}}^{\mathrm{W}}(\mathbf{x}(0), \mathbf{p}(0)) M_{\mathrm{DA}}^{\mathrm{W}}(\mathbf{x}(t), \mathbf{p}(t)) [\hat{H}_{\mathrm{I,DA}}]^{\mathrm{W}} (\mathbf{R}(t), \mathbf{P}(t)) \tag{14}$$

where $\mathbf{x} = (x_D, x_A)$ and $\mathbf{p} = (p_D, p_A)$ are the mapping variables arising from the QC/MH approach and $M_{\mathrm{DA}}^{\mathrm{W}}(\mathbf{x}, \mathbf{p})$ and $M_{\mathrm{AD}}^{\mathrm{W}}(\mathbf{x}, \mathbf{p})$ are the Wigner transforms in mapping variable space of $|\mathrm{D}\rangle\langle \mathrm{A}|$ and $|\mathrm{A}\rangle\langle \mathrm{D}|$, respectively. For an in-depth discussion of the different implementations of mapping variables that are possible for these operators, which give rise to the Ehrenfest, LSC I, and LSC II approaches discussed below, see refs 94−96 and section S1.5 of the Supporting Information.

Using the Wigner transform at time zero, $[\hat{H}_{\mathrm{I,AD}} \hat{\rho}_{\mathrm{D}}^{\mathrm{eq}}]^{\mathrm{W}} (\mathbf{R}(0), \mathbf{P}(0))$, which can be evaluated analytically for the model Hamiltonian under consideration, will be termed the Wigner of the product (WoP) approach. This time-zero Wigner transform can also be approximated, which has been termed the Wigner averaged classical limit (WACL) in previous work.[70,111] This approximation corresponds to applying the Wigner transform separately to each operator, such that

$$[\hat{H}_{\mathrm{I,AD}} \hat{\rho}_{\mathrm{D}}^{\mathrm{eq}}]^{\mathrm{W}} (\mathbf{R}(0), \mathbf{P}(0)) \approx [\hat{H}_{\mathrm{I,AD}}]^{\mathrm{W}} (\mathbf{R}(0), \mathbf{P}(0)) [\hat{\rho}_{\mathrm{D}}^{\mathrm{eq}}]^{\mathrm{W}} (\mathbf{R}(0), \mathbf{P}(0)) \tag{15}$$

which will be termed the product of Wigners (PoW) approach. Because both the partial and full linearization methods for calculating the FGR correlation function can be formulated in terms of the WoP or PoW approach, we will compare and contrast the performance of each of the four resulting approaches, which are illustrated in Figure 1. We note that the PoW formulation constitutes an approximation independent of the linearization scheme employed.

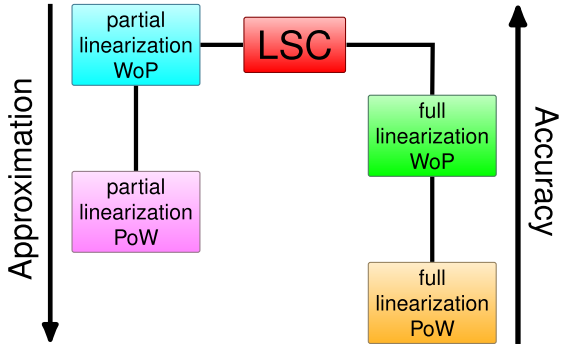

Figure 1. Schematic of LSC approximations to the equilibrium FGR rate constant.

Fully linearized results for the FGR correlation function were obtained by averaging over 10^6 trajectories, each consisting of 1000 time steps with a duration of 1 au each for a total simulation time of 1000 au. The initial conditions for the mapping variables were sampled from the Gaussian function arising from the Wigner transform of the coherence operators (see section S1.3 of the Supporting Information).[94−96] Initial coordinates and momenta for the photonic and nuclear DOF were sampled from the Wigner transform of the corresponding thermal equilibrium density operator (see section S1.3 of the Supporting Information). The quasiclassical equations of motion were integrated via diagonalization of the potential energy matrix at each time step.

Figure 2 shows CT rate constants, for model I (panel a) and Model II (panel b), obtained via partial linearization of the FGR correlation function, as per eq 11, eq S16 for WoP, and eq S21 for PoW. Unsurprisingly, the partially linearized LSC approximation within the WoP approach yields CT rate constants that coincide with the quantum-mechanically exact results, hence accurately predicting the cavity-free and cavity-enhanced CT rate constants and capturing the enhancement of the CT rate constant when the molecular system is placed inside a cavity. The distinction between the WoP and PoW approaches, however, becomes potentially important when the molecular system is placed inside the cavity. More specifically, the WoP partially linearized LSC expression for the FGR correlation function (eq 11) inside the cavity, which can be obtained in closed form for the model Hamiltonian in eq 1, can be analytically shown to coincide with the corresponding quantum-mechanically exact result (eq 9), which can also be obtained in closed form for this model Hamiltonian (see sections S2 and S3 of the Supporting Information). However, this is not the case for the PoW partially linearized approximation (see Figure 2). We note that in the cavity-free case, the fact that the donor−acceptor

https://doi.org/10.1021/acs.jpclett.2c00122
J. Phys. Chem. Lett. 2022, 13, 2330−2337

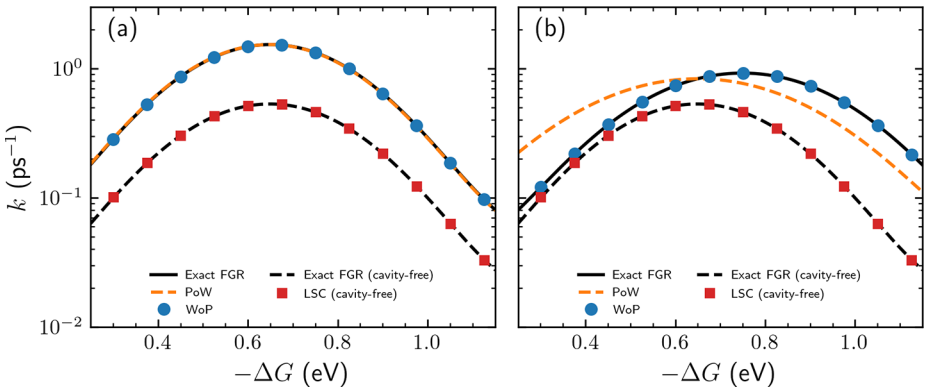

Figure 2. CT rate constants for (a) model I and (b) model II from partial linearization of the FGR correlation function, compared to exact FGR results.

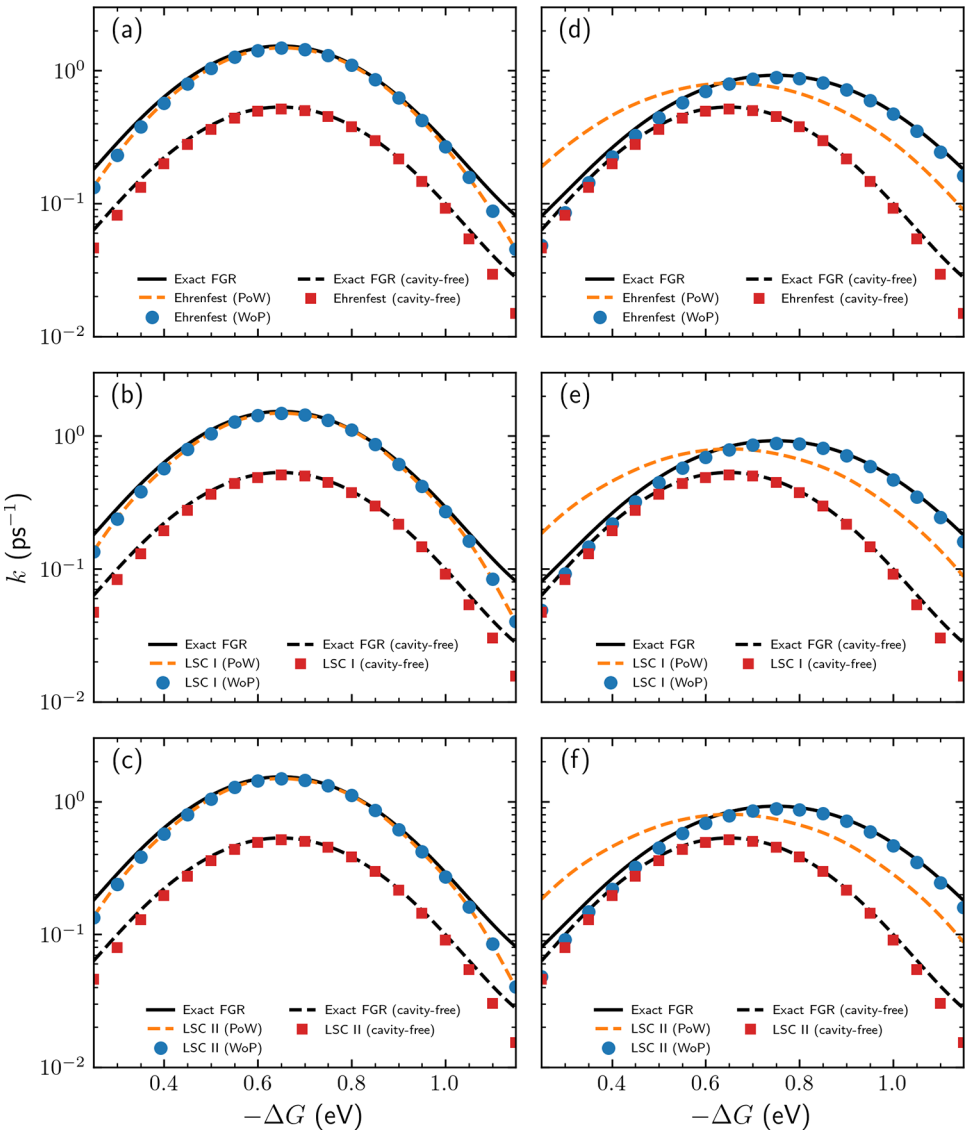

Figure 3. CT rate constants for (a−c) model I and (d−f) model II from full linearization of the FGR correlation function using the Ehrenfest, LSC I, and LSC II QC/MH methods, compared to exact FGR results.

coupling term is purely electronic makes the distinction between WoP and PoW obsolete.

Comparison between models I and II in fact highlights the difference between the formally exact WoP approach and the PoW approximation. For model I, shown in Figure 2a, the two strategies yield almost identical results. Conversely, for model II, shown in Figure 2b, which is characterized by a more quantum field mode and stronger light−matter coupling, the PoW approximation breaks down and yields considerable errors, up to an order of magnitude, in the CT rate constant.

https://doi.org/10.1021/acs.jpclett.2c00122
J. Phys. Chem. Lett. 2022, 13, 2330−2337

Figure 3 shows CT rate constants, for model I in panels a−c and model II in panels d−f, calculated via full linearization of the FGR correlation function, as per eq 14, obtained using three different QC/MH methods (Ehrenfest, LSC I, and LSC II).[94−96] Overall, full linearization also accurately predicts the cavity-free and cavity-enhanced CT rate constants and captures the enhancement of the CT rate constant when the molecular system is placed inside a cavity. Slight deviations from the formally exact partially linearized results can, however, be observed at larger driving forces, corresponding to the inverted regime, where one expects quantum nuclear/photonic effects to be more pronounced.[112,113]

Upon comparison of models I and II, the same breakdown of the PoW approximation in model II can be observed for full linearization. As in the case of the partial linearization results, errors in the rate constants obtained using the PoW approximation are considerable for model II, while the WoP approach maintains its excellent accuracy across both models I and II.

We note that Ehrenfest, LSC I, and LSC II yield almost identical fully linealized CT rate constants, which implies that the accuracy of the fully linearized approximation is insensitive to the choice of QC/MH method, at least for the model parameters under consideration. This is unsurprising, as the FGR correlation function contains only electronic coherences, the functional form of which is the same for all three methods. The only difference among the three QC/MH methods thus lies in the sampling of the initial conditions. In LSC I and LSC II, mapping variables are sampled from Gaussian functions of different widths,[94,95] while in the case of Ehrenfest, a focused sampling scheme is used.[103,104] Differences in how these methods approximate the FGR correlation function are therefore likely to manifest only for systems characterized by dynamics that explore a considerable extent of the electronic Hilbert space and require a broader sampling scheme as a result. Notably, this class of CT in a cavity system therefore constitutes a case in which the QC/MH methods investigated here are robust; i.e., one can obtain accurate results independent of one's choice of method for calculating the fully linearized FGR correlation function, provided the WoP strategy is applied.

The considerable and rapidly growing current interest in controlling molecular processes by coupling molecular matter to cavity modes[12−25,56] calls for accurate and scalable approximate methods for simulating the dynamics of chemical processes that take place in such systems. Methods based on classical-like trajectories show considerable promise in this regard.[67,68,70,71,82−104,114]

One such approach was recently considered by Huo et al., who demonstrated the ability of NRPMD (an approximate imaginary path integral method based on classical-like trajectories) to accurately capture the cavity-induced rate enhancement of CT reactions within the same model system under consideration in this paper.[105] In the case of ref 105, CT rate constants were estimated on the basis of simulating the relaxation dynamics of the donor population and fitting it to an exponential decay function. Huo et al. also showed that the same fitting procedure failed to yield accurate CT rate constants when the dynamics of the donor population was simulated within the framework of one possible implementation of the LSC approximation.

In this Letter, we have shown that it is in fact possible to obtain highly accurate CT rate constants, both inside and outside of a cavity, by applying the LSC approximation to the relatively short-lived FGR correlation function, as opposed to the relaxation dynamics of the donor population.

To this end, we compared and contrasted partially and fully linearized versions of LSC and showed that partial linearization not only is accurate but also is in fact formally exact for the same model system, both inside and outside the cavity, while full linearization is almost as accurate. We have also found that the accuracy of both partially and fully linearized versions of LSC relies on using the Wigner transform of the product of operators at the initial time (WoP), as opposed to the product of the corresponding Wigner transforms (PoW). We note that a similar conclusion regarding the role of WoP versus PoW was previously reached in the context of using LSC to calculate vibrational energy relaxation rate constants based on force−force correlation functions within the framework of the Landau−Teller formula.[69,115] We also note that situations in which WoP and PoW yield different results are also indicative of the sensitivity of the CT rate constant to nuclear and/or photonic dynamics (see section S4 of the Supporting Information).

Combining the LSC approximation with FGR rate theory can therefore provide a cost-effective, scalable, rigorous, and robust general purpose computational approach for estimating cavity-induced rate enhancement in CT reactions, as well as in other electronic transition processes that can be described by FGR rate theory. We note that a similar approach has recently been shown to be highly effective for calculating CT rate constants in a wide variety of complex cavity-free molecular systems.[110,116−118] The fact that placing the molecular system in a cavity amounts to adding a few nuclear-like photonic DOF, which are inherently harmonic and which couple only to the electronic dipole moment, suggests that such an approach will be as effective for similarly complex molecular systems placed inside cavities. Work on such extensions is currently underway and will be presented in future publications.

■ ASSOCIATED CONTENT

Supporting Information

The Supporting Information is available free of charge at https://pubs.acs.org/doi/10.1021/acs.jpclett.2c00122.

A detailed overview of the parameters, sampling of initial conditions, derivation of the closed form FGR expressions, a proof that the partially linearized LSC formulation of the WoP LSC expression yields the exact result, and an analysis of the sensitivity of the FGR correlation function to nuclear and photonic dynamics (PDF)

■ AUTHOR INFORMATION

Corresponding Author

Eitan Geva − *Department of Chemistry, University of Michigan, Ann Arbor, Michigan 48109, United States;* orcid.org/0000-0002-7935-4586; Email: eitan@umich.edu

Authors

Maximilian A. C. Saller − *Department of Chemistry, University of Michigan, Ann Arbor, Michigan 48109, United States*

Yifan Lai − *Department of Chemistry, University of Michigan, Ann Arbor, Michigan 48109, United States*

Complete contact information is available at: https://pubs.acs.org/10.1021/acs.jpclett.2c00122

Author Contributions

†M.A.C.S. and Y.L. contributed equally to this work.

Notes

The authors declare no competing financial interest.

■ ACKNOWLEDGMENTS

E.G. is grateful for support from the National Science Foundation via Grant CHE-1800325. This research was supported in part through computational resources and services provided by Advanced Research Computing-Technology Services (ARC-TS), a division of Information and Technology Services (ITS) at the University of Michigan.

■ REFERENCES

(1) Tannor, D. J.; Rice, S. A. Coherent Pulse Sequence Control of Product Formation in Chemical Reactions. *Adv. Chem. Phys.* **2007**, *70*, 441−523.
(2) Kosloff, R.; Rice, S. A.; Gaspard, P.; Tersigni, S.; Tannor, D. J. Wave Packet Dancing: Achieving Chemical Selectivity By Shaping Light Pulses. *Chem. Phys.* **1989**, *139*, 201−220.
(3) Gordon, R. J.; Rice, S. A. Active Control of The Dynamics of Atoms and Molecules. *Annu. Rev. Phys. Chem.* **1997**, *48*, 601−641.
(4) Assion, A.; Baumert, T.; Bergt, M.; Brixner, T.; Kiefer, B.; Seyfried, V.; Strehle, M.; Gerber, G. Control of Chemical Reactions by Feedback-Optimized Phase-Shaped Femtosecond Laser Pulses. *Science* **1998**, *282*, 919−922.
(5) Rabitz, H.; Zhu, W. Optimal Control of Molecular Motion: Design Implementation and Inversion. *Acc. Chem. Res.* **2000**, *33*, 572−578.
(6) Rice, S. A.; Zhao, M. *Optical Control of Molecular Dynamics*; Wiley: New York, 2000.
(7) Levis, R. J.; Menkir, G. M.; Rabitz, H. Selective Bond Dissociation and Rearrangement With Optimally Tailored Strong Field Laser Pulses. *Science* **2001**, *292*, 709−713.
(8) Pearson, B. J.; White, J. L.; Weinacht, T. C.; Bucksbaum, P. H. Coherent Control Using Adaptive Learning Algorithms. *Phys. Rev. A* **2001**, *63*, 063412.
(9) Rice, S. A.; Shah, S. P. Active Control of Product Selection in A Chemical Reaction: A View of The Current Scene. *Phys. Chem. Chem. Phys.* **2002**, *4*, 1683−1700.
(10) Shapiro, M.; Brumer, P. *Principles of the Quantum Control of Molecular Processes*; Wiley: Hoboken, NJ, 2002.
(11) McRobbie, P.; Geva, E. Coherent Control of Population Transfer via Linear Chirp in Liquid Solution: The Role of Motional Narrowing. *J. Phys. Chem. A* **2016**, *120*, 3015−3022.
(12) Lidzey, D.; Bradley, D.; Armitage, A.; Walker, S.; Skolnick, M. Photon-mediated hybridization of frenkel excitons in organic semiconductor microcavities. *Science* **2000**, *288*, 1620−1623.
(13) Tischler, J.; Bradley, M.; Bulović, V.; Song, J.; Nurmikko, A. Strong Coupling in a Microcavity LED. *Phys. Rev. Lett.* **2005**, *95*, 036401.
(14) Kéna-Cohen, S.; Davanço, M.; Forrest, S. Strong Exciton-Photon Coupling in an Organic Single Crystal Microcavity. *Phys. Rev. Lett.* **2008**, *101*, 116401.
(15) Kéna-Cohen, S.; Forrest, S. Room-temperature polariton lasing in an organic single-crystal microcavity. *Nat. Photonics* **2010**, *4*, 371−375.
(16) Hutchison, J.; Liscio, A.; Schwartz, T.; Canaguier-Durand, A.; Genet, C.; Palermo, V.; Samorì, P.; Ebbesen, T. Tuning the Work-Function Via Strong Coupling. *Adv. Mater.* **2013**, *25*, 2481−2485.
(17) Bellessa, J.; Symonds, C.; Laverdant, J.; Benoit, J.-M.; Plenet, J.; Vignoli, S. Strong Coupling between Plasmons and Organic Semiconductors. *Electronics* **2014**, *3*, 303−313.
(18) Schwartz, T.; Hutchison, J.; Genet, C.; Ebbesen, T. Reversible Switching of Ultrastrong Light-Molecule Coupling. *Phys. Rev. Lett.* **2011**, *106*, 196405−4.
(19) Kéna-Cohen, S.; Maier, S.; Bradley, D. Ultrastrongly Coupled Exciton-Polaritons in Metal-Clad Organic Semiconductor Microcavities. *Adv. Opt. Mater.* **2013**, *1*, 827−833.
(20) Mazzeo, M.; Genco, A.; Gambino, S.; Ballarini, D.; Mangione, F.; Di Stefano, O.; Patanè, S.; Savasta, S.; Sanvitto, D.; Gigli, G. Ultrastrong light-matter coupling in electrically doped microcavity organic light emitting diodes. *Appl. Phys. Lett.* **2014**, *104*, 233303−5.
(21) George, J.; Wang, S.; Chervy, T.; Canaguier-Durand, A.; Schaeffer, G.; Lehn, J.-M.; Hutchison, J.; Genet, C.; Ebbesen, T. Ultra-strong coupling of molecular materials: Spectroscopy and dynamics. *Faraday Discuss.* **2015**, *178*, 281−294.
(22) Dirac, P. A. M. *The principles of quantum mechanics*; Clarendon Press: Oxford, U.K., 1958.
(23) Louisell, W. H. *Radiation and Noise in Quantum Electronics*; McGraw-Hill: New York, 1964.
(24) Loudon, R. *The quantum theory of light*; Oxford University Press: New York, 1986.
(25) Walther, H.; Varcoe, B.; Englert, B.-G.; Becker, T. Cavity quantum electrodynamics. *Rep. Prog. Phys.* **2006**, *69*, 1325−1382.
(26) Andrew, P.; Barnes, W. L. Förster energy transfer in an optical microcavity. *Science* **2000**, *290*, 785−788.
(27) Hutchison, J.; Schwartz, T.; Genet, C.; Devaux, E.; Ebbesen, T. Modifying Chemical Landscapes by Coupling to Vacuum Fields. *Angew. Chem. Int.* **2012**, *51*, 1592−1596.
(28) Törmä, P.; Barnes, W. Strong coupling between surface plasmon polaritons and emitters: A review. *Rep. Prog. Phys.* **2015**, *78*, 013901−35.
(29) Flick, J.; Ruggenthaler, M.; Appel, H.; Rubio, A. Kohn−Sham approach to quantum electrodynamical density-functional theory: Exact time-dependent effective potentials in real space. *Proc. Natl. Acad. Sci. U.S.A.* **2015**, *112*, 15285−15290.
(30) Feist, J.; Garcia-Vidal, F. Extraordinary Exciton Conductance Induced by Strong Coupling. *Phys. Rev. Lett.* **2015**, *114*, 196402−5.
(31) Schachenmayer, J.; Genes, C.; Tignone, E.; Pupillo, G. Cavity-Enhanced Transport of Excitons. *Phys. Rev. Lett.* **2015**, *114*, 196403−6.
(32) Shalabney, A.; George, J.; Hutchison, J.; Pupillo, G.; Genet, C.; Ebbesen, T. Coherent coupling of molecular resonators with a microcavity mode. *Nat. Commun.* **2015**, *6*, 5981.
(33) Orgiu, E.; George, J.; Hutchison, J.; Devaux, E.; Dayen, J.; Doudin, B.; Stellacci, F.; Genet, C.; Schachenmayer, J.; Genes, C.; et al. Conductivity in organic semiconductors hybridized with the vacuum field. *Nat. Mater.* **2015**, *14*, 1123−1129.
(34) Long, J.; Simpkins, B. Coherent Coupling between a Molecular Vibration and Fabry−Perot Optical Cavity to Give Hybridized States in the Strong Coupling Limit. *ACS Photonics* **2015**, *2*, 130−136.
(35) Ebbesen, T. Hybrid Light−Matter States in a Molecular and Material Science Perspective. *Acc. Chem. Res.* **2016**, *49*, 2403−2412.
(36) Thomas, A.; George, J.; Shalabney, A.; Dryzhakov, M.; Varma, S.; Moran, J.; Chervy, T.; Zhong, X.; Devaux, E.; Genet, C.; et al. Ground-State Chemical Reactivity under Vibrational Coupling to the Vacuum Electromagnetic Field. *Angew. Chem.* **2016**, *128*, 11634−11638.
(37) Zhong, X.; Chervy, T.; Wang, S.; George, J.; Thomas, A.; Hutchison, J.; Devaux, E.; Genet, C.; Ebbesen, T. Non-Radiative Energy Transfer Mediated by Hybrid Light-Matter States. *Angew. Chem.* **2016**, *128*, 6310−6314.
(38) Herrera, F.; Spano, F. Cavity-Controlled Chemistry in Molecular Ensembles. *Phys. Rev. Lett.* **2016**, *116*, 238301−6.
(39) Casey, S.; Sparks, J. Vibrational Strong Coupling of Organometallic Complexes. *J. Phys. Chem. C* **2016**, *120*, 28138−28143.
(40) Sanvitto, D.; Kéna-Cohen, S. The road towards polaritonic devices. *Nat. Mater.* **2016**, *15*, 1061−1073.
(41) Kowalewski, M.; Bennett, K.; Mukamel, S. Cavity Femtochemistry: Manipulating Nonadiabatic Dynamics at Avoided Crossings. *J. Phys. Chem. Lett.* **2016**, *7*, 2050−2054.
(42) Kowalewski, M.; Bennett, K.; Mukamel, S. Non-adiabatic dynamics of molecules in optical cavities. *J. Chem. Phys.* **2016**, *144*, 054309−9.
(43) Flick, J.; Ruggenthaler, M.; Appel, H.; Rubio, A. Atoms and molecules in cavities, from weak to strong coupling in quantum-

https://doi.org/10.1021/acs.jpclett.2c00122
J. Phys. Chem. Lett. 2022, 13, 2330−2337

electrodynamics (QED) chemistry. *Proc. Natl. Acad. Sci. U.S.A.* **2017**, *114*, 3026−3034.
(44) Zhong, X.; Chervy, T.; Zhang, L.; Thomas, A.; George, J.; Genet, C.; Hutchison, J.; Ebbesen, T. Energy Transfer between Spatially Separated Entangled Molecules. *Angew. Chem., Int. Ed.* **2017**, *56*, 9034−9038.
(45) Martínez-Martínez, L.; Ribeiro, R.; Campos-González-Angulo, J.; Yuen-Zhou, J. Can Ultrastrong Coupling Change Ground-State Chemical Reactions? *ACS Photonics* **2018**, *5*, 167−176.
(46) Fregoni, J.; Granucci, G.; Coccia, E.; Persico, M.; Corni, S. Manipulating azobenzene photoisomerization through strong light-molecule coupling. *Nat. Commun.* **2018**, *9*, 4688.
(47) Sáez-Blázquez, R.; Feist, J.; Fernández-Domínguez, A.; García-Vidal, F. Organic polaritons enable local vibrations to drive long-range energy transfer. *Phys. Rev. B* **2018**, *97*, 241407−5.
(48) Flick, J.; Welakuh, D.; Ruggenthaler, M.; Appel, H.; Rubio, A. Light−Matter Response in Nonrelativistic Quantum Electrodynamics. *ACS Photonics* **2019**, *6*, 2757−2778.
(49) Galego, J.; Climent, C.; Garcia-Vidal, F.; Feist, J. Cavity Casimir-Polder Forces and Their Effects in Ground-State Chemical Reactivity. *Phys. Rev. X* **2019**, *9*, 021057−22.
(50) Lather, J.; Bhatt, P.; Thomas, A.; Ebbesen, T.; George, J. Cavity Catalysis by Cooperative Vibrational Strong Coupling of Reactant and Solvent Molecules. *Angew. Chem., Int. Ed.* **2019**, *58*, 10635−10638.
(51) Schäfer, C.; Ruggenthaler, M.; Appel, H.; Rubio, A. Modification of excitation and charge transfer in cavity quantum-electrodynamical chemistry. *Proc. Natl. Acad. Sci. U.S.A.* **2019**, *116*, 4883−4892.
(52) Hoffmann, N.; Schäfer, C.; Rubio, A.; Kelly, A.; Appel, H. Capturing vacuum fluctuations and photon correlations in cavity quantum electrodynamics with multitrajectory Ehrenfest dynamics. *Phys. Rev. A* **2019**, *99*, 063819−9.
(53) Hoffmann, N.; Schäfer, C.; Säkkinen, N.; Rubio, A.; Appel, H.; Kelly, A. Benchmarking semiclassical and perturbative methods for real-time simulations of cavity-bound emission and interference. *J. Chem. Phys.* **2019**, *151*, 244113−14.
(54) Lacombe, L.; Hoffmann, N.; Maitra, N. Exact Potential Energy Surface for Molecules in Cavities. *Phys. Rev. Lett.* **2019**, *123*, 083201−6.
(55) Mandal, A.; Huo, P. Investigating New Reactivities Enabled by Polariton Photochemistry. *J. Phys. Chem. Lett.* **2019**, *10*, 5519−5529.
(56) Semenov, A.; Nitzan, A. Electron transfer in confined electromagnetic fields. *J. Chem. Phys.* **2019**, *150*, 174122.
(57) Hoffmann, N.; Lacombe, L.; Rubio, A.; Maitra, N. Effect of Many Modes on Self-Polarization and Photochemical Suppression in Cavities. *J. Chem. Phys.* **2020**, *153*, 104103.
(58) Flick, J.; Rivera, N.; Narang, P. Strong light-matter coupling in quantum chemistry and quantum photonics. *Nanophotonics* **2018**, *7*, 1479−1501.
(59) Gu, B.; Mukamel, S. Manipulating nonadiabatic conical intersection dynamics by optical cavities. *Chem. Sci.* **2020**, *11*, 1290−1298.
(60) Mandal, A.; Krauss, T.; Huo, P. Polariton-Mediated Electron Transfer via Cavity Quantum Electrodynamics. *J. Phys. Chem. B* **2020**, *124*, 6321−6340.
(61) Saller, M. A. C.; Kelly, A.; Geva, E. Benchmarking Quasiclassical Mapping Hamiltonian Methods for Simulating Cavity-Modified Molecular Dynamics. *J. Phys. Chem. Lett.* **2021**, *12*, 3163−3170.
(62) Dicke, R. Coherence in spontaneous radiation processes. *Phys. Rev.* **1954**, *93*, 99−110.
(63) Jaynes, E.; Cummings, F. Comparison of quantum and semiclassical radiation theories with application to the beam maser. *Proc. IEEE* **1963**, *51*, 89−109.
(64) Tavis, M.; Cummings, F. Approximate solutions for an N-molecule-radiation-field Hamiltonian. *Phys. Rev.* **1969**, *188*, 692−695.
(65) Houdre, R.; Stanley, R.; Ilegems, M. Vacuum-field Rabi splitting in the presence of inhomogeneous broadening: Resolution of a homogeneous linewidth in an inhomogeneously broadened system. *Phys. Rev. A* **1996**, *53*, 2711−2715.
(66) Garraway, B. The Dicke model in quantum optics: Dicke model revisited. *P. R. Soc. A: Math. Phys.* **2011**, *369*, 1137−1155.
(67) Wang, H.; Thoss, M.; Miller, W. H. Forward-backward initial value representation for the calculation of thermal rate constants for reactions in complex molecular systems. *J. Chem. Phys.* **2000**, *112*, 47−55.
(68) Shi, Q.; Geva, E. A relationship between semiclassical and centroid correlation functions. *J. Chem. Phys.* **2003**, *118*, 8173−8184.
(69) Shi, Q.; Geva, E. A semiclassical theory of vibrational energy relaxation in the condensed phase. *J. Phys. Chem. A* **2003**, *107*, 9059−9069.
(70) Shi, Q.; Geva, E. Nonradiative electronic relaxation rate constants from approximations based on linearizing the path-integral forward-backward action. *J. Phys. Chem. A* **2004**, *108*, 6109−6116.
(71) Shi, Q.; Geva, E. A semiclassical generalized quantum master equation for an arbitrary system-bath coupling. *J. Chem. Phys.* **2004**, *120*, 10647−10658.
(72) Shi, Q.; Geva, E. A derivation of the mixed quantum-classical Liouville equation from the influence functional formalism. *J. Chem. Phys.* **2004**, *121*, 3393−3404.
(73) Sun, X.; Geva, E. Equilibrium Fermi's Golden Rule Charge Transfer Rate Constants in the Condensed Phase: The Linearized Semiclassical Method vs Classical Marcus Theory. *J. Phys. Chem. A* **2016**, *120*, 2976−2990.
(74) Huo, P.; Coker, D. Communication: Partial linearized density matrix dynamics for dissipative, non-adiabatic quantum evolution. *J. Chem. Phys.* **2011**, *135*, 201101−4.
(75) Huo, P.; Coker, D. Semi-classical path integral non-adiabatic dynamics: a partial linearized classical mapping Hamiltonian approach. *Mol. Phys.* **2012**, *110*, 1035−1052.
(76) Huo, P.; Coker, D. Consistent schemes for non-adiabatic dynamics derived from partial linearized density matrix propagation. *J. Chem. Phys.* **2012**, *137*, 22A535−19.
(77) Huo, P.; Miller, T. F., III; Coker, D. F. Predictive partial linearized path integral simulation of condensed phase electron transfer dynamics. *J. Chem. Phys.* **2013**, *139*, 151103−4.
(78) Bonella, S.; Ciccotti, G.; Kapral, R. Linearization approximations and Liouville quantum−classical dynamics. *Chem. Phys. Lett.* **2010**, *484*, 399−404.
(79) Sun, X.; Geva, E. Nonequilibrium Fermi's Golden Rule Charge Transfer Rates via the Linearized Semiclassical Method. *J. Chem. Theory Comput.* **2016**, *12*, 2926−2941.
(80) Sun, X.; Geva, E. Non-Condon Equilibrium Fermi's Golden Rule Electronic Transition Rate Constants Via The Linearized Semiclassical Method. *J. Chem. Phys.* **2016**, *144*, 244105−12.
(81) Sun, X.; Geva, E. Non-Condon nonequilibrium Fermi's golden rule rates from the linearized semiclassical method. *J. Chem. Phys.* **2016**, *145*, 064109−19.
(82) Stock, G.; Thoss, M. Classical description of nonadiabatic quantum dynamics. *Adv. Chem. Phys.* **2005**, *131*, 243−376.
(83) Meyer, H.-D.; Miller, W. A classical analog for electronic degrees of freedom in nonadiabatic collision processes. *J. Chem. Phys.* **1979**, *70*, 3214−3223.
(84) Stock, G.; Thoss, M. Semiclassical Description of Nonadiabatic Quantum Dynamics. *Phys. Rev. Lett.* **1997**, *78*, 578−581.
(85) Sun, X.; Wang, H.; Miller, W. Semiclassical theory of electronically nonadiabatic dynamics: Results of a linearized approximation to the initial value representation. *J. Chem. Phys.* **1998**, *109*, 7064.
(86) Wang, H.; Song, X.; Chandler, D.; Miller, W. Semiclassical study of electronically nonadiabatic dynamics in the condensed phase: Spin-boson problem with Debye spectral density. *J. Chem. Phys.* **1999**, *110*, 4828−4840.
(87) Swenson, D.; Levy, T.; Cohen, G.; Rabani, E.; Miller, W. Application of a semiclassical model for the second-quantized many-electron Hamiltonian to nonequilibrium quantum transport: The resonant level model. *J. Chem. Phys.* **2011**, *134*, 164103−9.
(88) Cotton, S.; Miller, W. Symmetrical windowing for quantum states in quasi-classical trajectory simulations: Application to electronically non-adiabatic processes. *J. Chem. Phys.* **2013**, *139*, 234112−10.

https://doi.org/10.1021/acs.jpclett.2c00122
J. Phys. Chem. Lett. 2022, 13, 2330−2337

(89) Cotton, S.; Miller, W. Symmetrical Windowing for Quantum States in Quasi-Classical Trajectory Simulations. *J. Phys. Chem. A* **2013**, *117*, 7190−7194.
(90) Cotton, S.; Igumenshchev, K.; Miller, W. Symmetrical windowing for quantum states in quasi-classical trajectory simulations: Application to electron transfer. *J. Chem. Phys.* **2014**, *141*, 084104−11.
(91) Cotton, S.; Miller, W. A Symmetrical Quasi-Classical Spin-Mapping Model for the Electronic Degrees of Freedom in Non-Adiabatic Processes. *J. Phys. Chem. A* **2015**, *119*, 12138−12145.
(92) Cotton, S.; Miller, W. The Symmetrical Quasi-Classical Model for Electronically Non-Adiabatic Processes Applied to Energy Transfer Dynamics in Site-Exciton Models of Light-Harvesting Complexes. *J. Chem. Theory Comput.* **2016**, *12*, 983−991.
(93) Cotton, S.; Miller, W. A new symmetrical quasi-classical model for electronically non-adiabatic processes: Application to the case of weak non-adiabatic coupling. *J. Chem. Phys.* **2016**, *145*, 144108−17.
(94) Saller, M.; Kelly, A.; Richardson, J. On the identity of the identity operator in nonadiabatic linearized semiclassical dynamics. *J. Chem. Phys.* **2019**, *150*, 071101−8.
(95) Saller, M.; Kelly, A.; Richardson, J. Improved population operators for multi-state nonadiabatic dynamics with the mixed quantum-classical mapping approach. *Faraday Discuss.* **2020**, *221*, 150−167.
(96) Gao, X.; Saller, M.; Liu, Y.; Kelly, A.; Richardson, J.; Geva, E. Benchmarking Quasiclassical Mapping Hamiltonian Methods for Simulating Electronically Nonadiabatic Molecular Dynamics. *J. Chem. Theory Comput.* **2020**, *16*, 2883−2895.
(97) Tao, G. Electronically Nonadiabatic Dynamics in Singlet Fission: A Quasi-Classical Trajectory Simulation. *J. Phys. Chem. C* **2014**, *118*, 17299−17305.
(98) Tao, G. A multi-state trajectory method for non-adiabatic dynamics simulations. *J. Chem. Phys.* **2016**, *144*, 094108−9.
(99) Tao, G.; Shen, N. Mapping State Space to Quasiclassical Trajectory Dynamics in Coherence-Controlled Nonadiabatic Simulations for Condensed Phase Problems. *J. Phys. Chem. A* **2017**, *121*, 1734−1747.
(100) Tao, G. Nonadiabatic Dynamics of Hydrogen Diffusion on Cu(001): Classical Mapping Model with Multistate Projection Window in Real Space. *ChemPhysChem* **2019**, *62*, 2127−2135.
(101) Liu, J. A unified theoretical framework for mapping models for the multi-state Hamiltonian. *J. Chem. Phys.* **2016**, *145*, 204105−15.
(102) He, X.; Liu, J. A new perspective for nonadiabatic dynamics with phase space mapping models. *J. Chem. Phys.* **2019**, *151*, 024105−22.
(103) Runeson, J.; Richardson, J. Spin-mapping approach for nonadiabatic molecular dynamics. *J. Chem. Phys.* **2019**, *151*, 044119−14.
(104) Runeson, J. E.; Richardson, J. O. Generalized spin mapping for quantum-classical dynamics. *J. Chem. Phys.* **2020**, *152*, 084110.
(105) Chowdhury, S. N.; Mandal, A.; Huo, P. Ring polymer quantization of the photon field in polariton chemistry. *J. Chem. Phys.* **2021**, *154*, 044109.
(106) Richardson, J.; Thoss, M. Communication: Nonadiabatic ring-polymer molecular dynamics. *J. Chem. Phys.* **2013**, *139*, 031102−3.
(107) Richardson, J.; Meyer, P.; Pleinert, M.-O.; Thoss, M. An analysis of nonadiabatic ring-polymer molecular dynamics and its application to vibronic spectra. *Chem. Phys.* **2017**, *482*, 124−134.
(108) Chowdhury, S. N.; Huo, P. State dependent ring polymer molecular dynamics for investigating excited nonadiabatic dynamics. *J. Chem. Phys.* **2019**, *150*, 244102.
(109) Makri, N. The Linear Response Approximation and Its Lowest Order Corrections: An Influence Functional Approach. *J. Phys. Chem. B* **1999**, *103*, 2823−2829.
(110) Sun, X.; Zhang, P.; Lai, Y.; Williams, K.; Cheung, M.; Dunietz, B.; Geva, E. Computational Study of Charge-Transfer Dynamics in the Carotenoid-Porphyrin-C_{60} Molecular Triad Solvated in Explicit Tetrahydrofuran and Its Spectroscopic Signature. *J. Phys. Chem. C* **2018**, *122*, 11288−11299.
(111) Egorov, S. A.; Rabani, E.; Berne, B. J. Nonradiative relaxation processes in condensed phases: Quantum vs. classical baths. *J. Chem. Phys.* **1999**, *110*, 5238−5248.
(112) Barbara, P. F.; Meyer, T. J.; Ratner, M. A. Contemporary Issues in Electron Transfer Research. *J. Phys. Chem.* **1996**, *100*, 13148−13168.
(113) Lee, M. H.; Dunietz, B. D.; Geva, E. Calculation From First Principles of Intramolecular Golden-Rule Rate Constants for Photo-Induced Electron Transfer in Molecular Donor-Acceptor Systems. *J. Phys. Chem. C* **2013**, *117*, 23391−23401.
(114) McLachlan, A. A variational solution of the time-dependent Schrodinger equation. *Mol. Phys.* **1964**, *8*, 39−44.
(115) Shi, Q.; Geva, E. Vibrational energy relaxation in liquid oxygen from a semiclassical molecular dynamics simulation. *J. Phys. Chem. A* **2003**, *107*, 9070−9078.
(116) Han, J.; Zhang, P.; Aksu, H.; Maiti, B.; Sun, X.; Geva, E.; Dunietz, B.; Cheung, M. S. On the Interplay Between Electronic Structure and Polarizable Force Fields When Calculating Solution-Phase Charge Transfer Rates. *J. Chem. Theory Comput.* **2020**, *16*, 6481−6490.
(117) Tinnin, J.; Bhandari, S.; Zhang, P.; Aksu, H.; Maiti, B.; Geva, E.; Dunietz, B. D.; Sun, X.; Cheung, M. S. Molecular-Level Exploration of the Structure-Function Relations Underlying Interfacial Charge Transfer in the Subphthalocyanine/C_{60} Organic Photovoltaic System. *Phys. Rev. Applied* **2020**, *13*, 054075.
(118) Tinnin, J.; Aksu, H.; Tong, Z.; Zhang, P.; Geva, E.; Dunietz, B. D.; Sun, X.; Cheung, M. S. CTRAMER: An open-source software package for correlating interfacial charge transfer rate constants with donor/acceptor geometries in organic photovoltaic materials. *J. Chem. Phys.* **2021**, *154*, 214108.

https://doi.org/10.1021/acs.jpclett.2c00122
J. Phys. Chem. Lett. 2022, 13, 2330−2337